markers of *Y. enterocolitica* pathogenicity[14]. However, recent studies have shown that biotype 1A strains produce heat stable enterotoxin[15], invade cultured epithelial cells[16] and resist killing by macrophages[17]. *Y. enterocolitica* serotype O : 6,30 belonging to biotype 1A, observed in this study, has been implicated in nosocomial and milk-borne outbreaks in certain parts of the world[18]. This serotype has also been isolated from extraintestinal infections in human beings[19]. All these observations point to its pathogenic potential. This serotype has not been reported earlier from India.

The present study provides a report of isolation of *Y. enterocolitica* from swine oral swab, groundwater and surface water in India. The isolation of *Y. intermedia* and *Y. frederiksenii* from human diarrhoeic stools, and *Y. intermedia* from swine also represents their first isolation from these sources in India. The clinical significance of *Y. intermedia* and *Y. frederiksenii* is controversial[20] and further studies are awaited in this aspect. Some of the atypical biochemical characteristics especially lactose positivity of *Y. intermedia* and nitrate negativity of *Y. frederiksenii* isolates were noteworthy. It would be worthwhile to work on the prevalence of *Y. enterocolitica* in human, animals and environment in this part of the continent.

1. Ostroff, S., *Contrib. Microbiol. Immunol.*, 1995, **13**, 5–10.
2. Bottone, E. J., *Microbes Infect.*, 1999, **1**, 323–333.
3. Abraham, M., Pai, M., Kang, G., Asokan, G. V., Magesh, S. R., Bhattacharji, S. and Ramakrishna, B. S., *Indian J. Med. Res.*, 1997, **106**, 465–468.
4. Pramanik, A. K., Bhattacharyya, H. M., Chatterjee, A. and Sengupta, D. N., *Indian J. Anim. Health*, 1980, **19**, 79–81.
5. Singh, G., Arora, N. K., Bhan, M. K., Ghai, O. P., Dhar, S. and Shriniwas, *Indian J. Pediatr.*, 1983, **50**, 39–42.
6. Varghese, A., Ramachandran, V. G. and Agarwal, D. S., *Indian J. Med. Res.*, 1984, **79**, 35–40.
7. Ram, S., Khurana, S., Singh, R., Sharma, S. and Vadehra, D. V., *Indian J. Med. Res.*, 1987, **86**, 9–13.
8. Toora, S., Bala, A. S., Tiwari, R. P. and Singh, G., *Folia Microbiol.*, 1989, **34**, 151–156.
9. Verma, N. K. and Misra, D. S., *Indian J. Anim. Sci.*, 1984, **54**, 659–662.
10. Singh, I. and Virdi, J. S., *Curr. Sci.*, 1999, **77**, 1019–1021.
11. Sinha, I., Choudhary, I. and Virdi, J. S., *Curr. Sci.*, 2000, **79**, 510–513.
12. Schiemann, D. A., *Can. J. Microbiol.*, 1979, **25**, 1298–1304.
13. Barrow, G. I. and Feltham, R. K. A. (eds), *Cowan and Steel's Manual for Identification of Medical Bacteria*, Cambridge University Press, Cambridge, 1993, 3rd edn, pp. 94–164.
14. Burnens, A. P., Frey, A. and Nicolet, J., *Epidemiol. Infect.*, 1996, **116**, 27–34.
15. Robins-Browne, R. M. *et al.*, *Infect. Immun.*, 1993, **61**, 764–767.
16. Grant, T., Bennett-Wood, V. and Robins-Browne, R. M., *Infect. Immun.*, 1998, **66**, 1113–1120.
17. Grant, T., Bennett-Wood, V. and Robins-Browne, R. M., *Infect. Immun.*, 1999, **67**, 4367–4375.
18. Greenwood, M. H. and Hooper, W. L., *Epidemiol. Infect.*, 1990, **104**, 345–350.
19. Bissett, M. L., Powers, C., Abbott, S. L. and Janda, J. M., *J. Clin. Microbiol.*, 1990, **28**, 910–912.
20. Sulakvelidze, A., *Microbes Infect.*, 2000, **2**, 497–513.

ACKNOWLEDGEMENTS. We thank Dr M. K. Bhan and members of ORU and DTU unit for their help in collection of clinical samples. We thank Dr Elisabeth Carniel, Director, WHO *Yersinia* Reference Center, Pasteur Institute, Paris for serotyping of clinical isolates. The study was supported by ICMR-SRF to I.S. and by a research project of DST to J.S.V.

Received 4 October 2002; revised accepted 7 January 2003

Microstructural and fluid inclusion constraints on the evolution of Jakhri Thrust Zone in the Satluj valley of NW Himalaya

A. K. Pandey* and N. S. Virdi

Wadia Institute of Himalayan Geology, Dehra Dun 248 001, India

The regional structures, microstructure and fluid inclusion trail pattern have been employed to work out the evolution of the Jakhri Thrust Zone (JTZ) exposed in the Satluj valley of NW Himalaya. It is a NE-dipping, SW-propagating out-of-sequence thrust cutting across the folded Lesser Himalayan crystalline nappe and lies in the seismically active inner Lesser Himalayan zone. The recrystallization microstructure in the footwall quartzite suggests deformation in the lower green schist facies condition with a progressively decreasing finite strain away from the thrust. The microstructures and fluid inclusion trails (secondary) show analogous pattern and have formed during the same deformation event in the footwall. The CO_2–H_2O and H_2O–NaCl fluid inclusions have been identified. The former has been re-equilibrated during the peak deformation whereas the latter has evolved and been re-equilibrated during exhumation. The isochores of CO_2–H_2O and H_2O–NaCl inclusions suggest an isothermal exhumation path from a depth of ~15–17 km, considering a lithostatic condition. These results suggest that the JTZ is a deep-seated thrust, probably a steep imbrication on the main decollement fault.

THE Jakhri Thrust Zone (JTZ) lies in the Satluj valley of NW-Himalaya (Figure 1). The tectonic status of the JTZ is debated and recent fission track data on zircon–apatite cogenetic pairs from the hanging wall of the JTZ suggest it to be active during past < 4.5 Ma (ref. 1), which is younger than the age MBT, i.e. ca. 10 Ma (ref. 2). The

*For correspondence. (e-mail: anandkumarpandey@rediffmail.com)

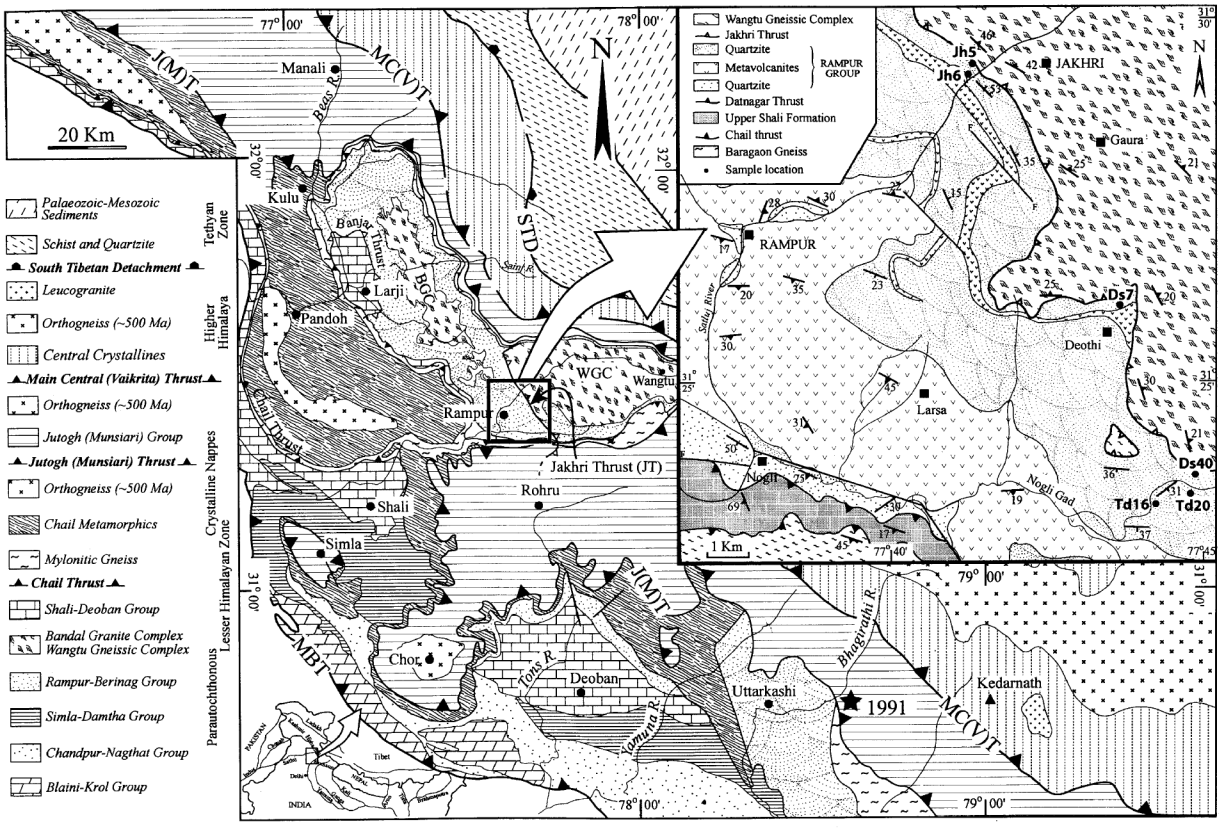

Figure 1. Regional geological map of a part of Western Himalaya showing the extent of Kulu–Rampur and Larji window zone and the position of Jakhri Thrust. The inset map shows detailed geology of the study area and sample location. (Compiled and modified from refs 16, 17 and 19 and our own observations. STD, South Tibetan Detachment; MC(V)T, Main Central (Vaikrita) Thrust; J(M)T, Jutogh (Munsiari) Thrust; MBT, Main Boundary Thrust; BGC, Bandal Granite Complex; WGC, Wangtu Gneissic Complex).

oxygen isotope thermometry in the hanging wall of the JTZ suggests ~600°C peak temperature in the immediate vicinity of the thrust[3]. In the present study, microstructures in the JTZ aided by fluid inclusion studies in the footwall quartzite have been used to delineate the exhumation history of the JTZ. Many studies[4–7] have indicated that the fluid inclusion trails are related to specific deformation events and their geometry can be a useful parameter in dealing with the tectonic studies. They have been used in dealing with the exhumation history of the Higher Himalaya, as well[8–11]. The fluid inclusion study has been performed on the footwall quartzite as it preserves the complete deformation history, particularly after peak deformation. The extent of the effect of thrusting has been constrained by the ductile microstructures. The microstructures and fluid inclusion trails geometry suggest they are genetically related. The microthermometric measurements on these fluid inclusions have been used to constrain *PT* evolution during exhumation.

The parautochthonous Rampur Group, constituted of quartzite and 1800 ± 13 Ma-old metavolcanites[12], and 1895 ± 64 Ma-old Wangtu Gneissic Complex (WGC)[13] exposed in the Kulu–Rampur window in the NW Himalaya (Figure 1). The WGC has been considered to be equivalent to the Bandal Granite Complex (BGC) based on lithological similarity, tectonic position and age, viz. 1800 ± 70 Ma (ref. 14) and 1840 ± 16 Ma (ref. 12) for BGC. The parautochthons are tectonically overlain by the Lesser Himalayan Crystallines, viz. Chail and Jutogh (Munsiari) nappes. In the Satluj valley the WGC is thrusted on the Rampur quartzite along the JTZ (Figure 1) with ~4 km wide mylonitic zone in the hanging wall and ~1–1.5 km in the footwall. The tectonic status of the JTZ has been debated. One view considers JTZ as part of Jutogh (Munsiari) Thrust[15,16] and therefore has a regional tectonic significance. However, Bhargava[17] considers the JTZ as a local tectonic boundary with a limited lateral extent within the Kulu–Rampur window zone.

The rocks in the Rampur window zone have suffered multiple deformation[18,19]. The axial plane cleavage S_1 forms the prominent foliation and can only be distinguished from S_0 in the hinge zones of isoclinal F_1. The F_1 folding is followed by south propagating (D_2) regional thrusting along Jutogh (Munsiari) Thrust, which in turn is followed by regional F_3 and F_4 folding. This is evident from the folded D_2 thrusts (Figures 1 and 2 *a*). The JTZ,

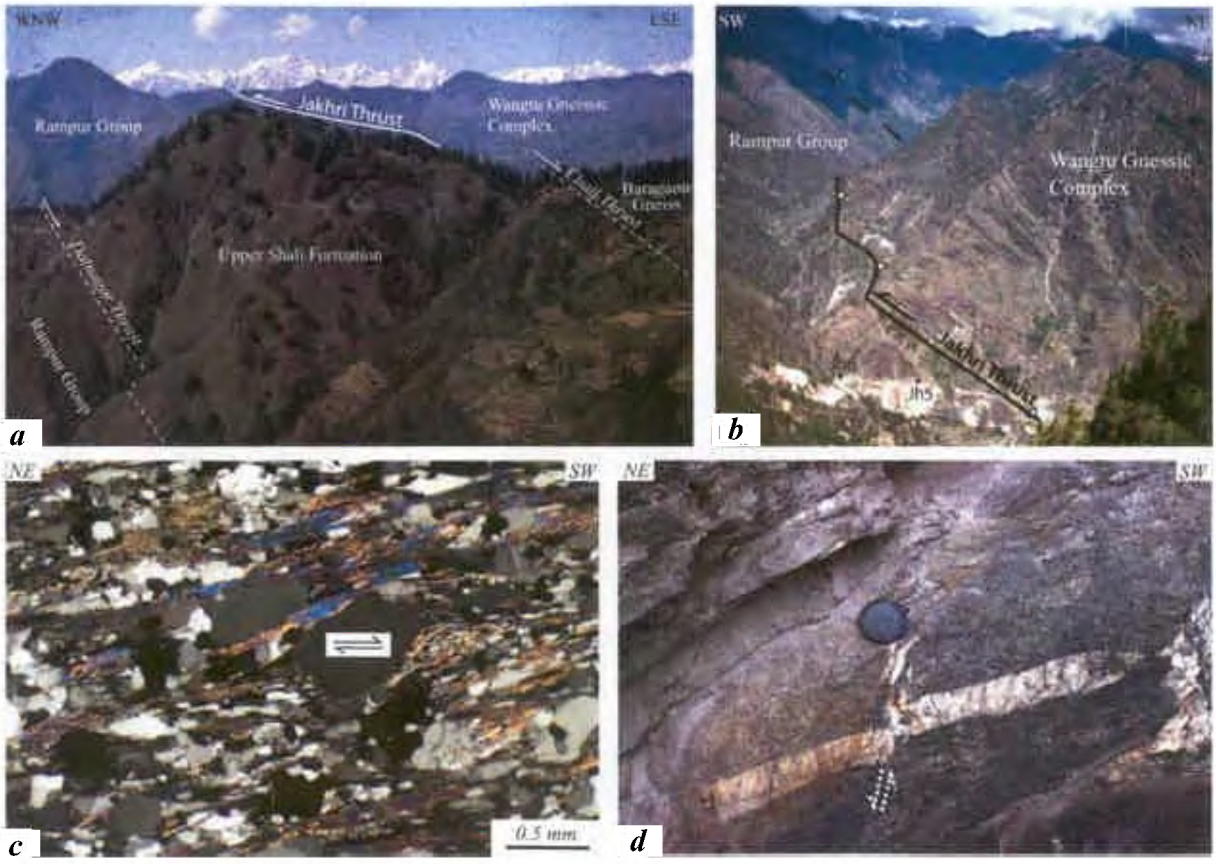

Figure 2. ***a***, NE dipping Jakhri Thrust cutting across the SW dipping folded (F_3) Chail and Datnagar thrusts; ***b***, The outcrop view of the NE dipping Jakhri Thrust with WGC constituting hanging wall and Rampur Group in the foot wall; ***c***, The σ-type asymmetric strain shadow around feldspar porphyroclast in the mylonitic orthogneisses of WGC, suggesting top to SW shearing in the hanging wall of the JTZ; ***d***, Extensional fault deforming the quartz vein with apparent top to NE shearing in the hanging wall of the JTZ. Also note the quartz-filled tension gashes parallel to the fault.

along which the WGC has exhumation, dips ~ 50° due NE (Figure 2 *b*) and cuts across the regional F_3 (Figures 1 and 2 *a*).

The well-developed S–C fabric, deformed quartz ribbon, σ-type asymmetric strain shadow around feldspar porphyroclasts (Figure 2 *c*) and asymmetrically boudinaged quartz lenses in the hanging wall suggest top to SW thrusting along the JTZ. The extensional fault with fault parallel tension gashes (Figure 2 *d*) and pull-apart microstructure in the quartz porphyroclasts oblique to foliation marks the post-thrusting top to NE sub-vertical extensional shearing in the hanging wall. The steep bending of footwall foliation (S_1 and C) and slikensides in the immediate vicinity of the thrust also suggest the same.

In the footwall of the JTZ, antithetically faulted quartzite pebbles (Figure 3 *a*) and semi-brittle shear zones (Figure 3 *b*) with top to SW shearing have been observed. The microstructures in the quartzite show decrease in shape-preferred alignment of quartz grains and an increase in porphyroclastic quartz content (Figure 3 *c*, *d*) with increasing distance from the JT. In the immediate vicinity of the JTZ, the quartzite is fine-grained (~ 100 μm) and intensely recrystallized showing shape-preferred alignment. Quartz-ribbons forming oblique foliation (S_1) tend to become parallel to shear foliation (C) suggesting top to SW shearing (Figure 3 *c*). In the intermediate zone, quartzite is constituted of quartz porphyroclasts (< 3 mm) in recrystallized quartz (~ 100 μm), chlorite and sericite matrix. Subgrains are well-developed in quartz porphyroclasts and sutured subgrain boundary suggests that grain boundary migration is the main mode of recrystallization. In the farthest zone, the porphyroclastic quartz (< 3 mm) with core and mantle structure (Figure 3 *d*) constitutes the quartzite. The strain lamellae in quartz lie roughly parallel to the grain alignment direction.

The fluids entrapped in the healed microcracks are observed in the form of Fluid Inclusion Plane (FIP) and they have been used as paleostress indicators[5,10]. They also suggest that the rock may behave in a brittle manner even under ductile deformation condition due to strain incompatibility and sliding between neighbouring grains[7]. With this background, the fluid inclusion trail (2-D analog of fluid inclusion plane) patterns have been measured with

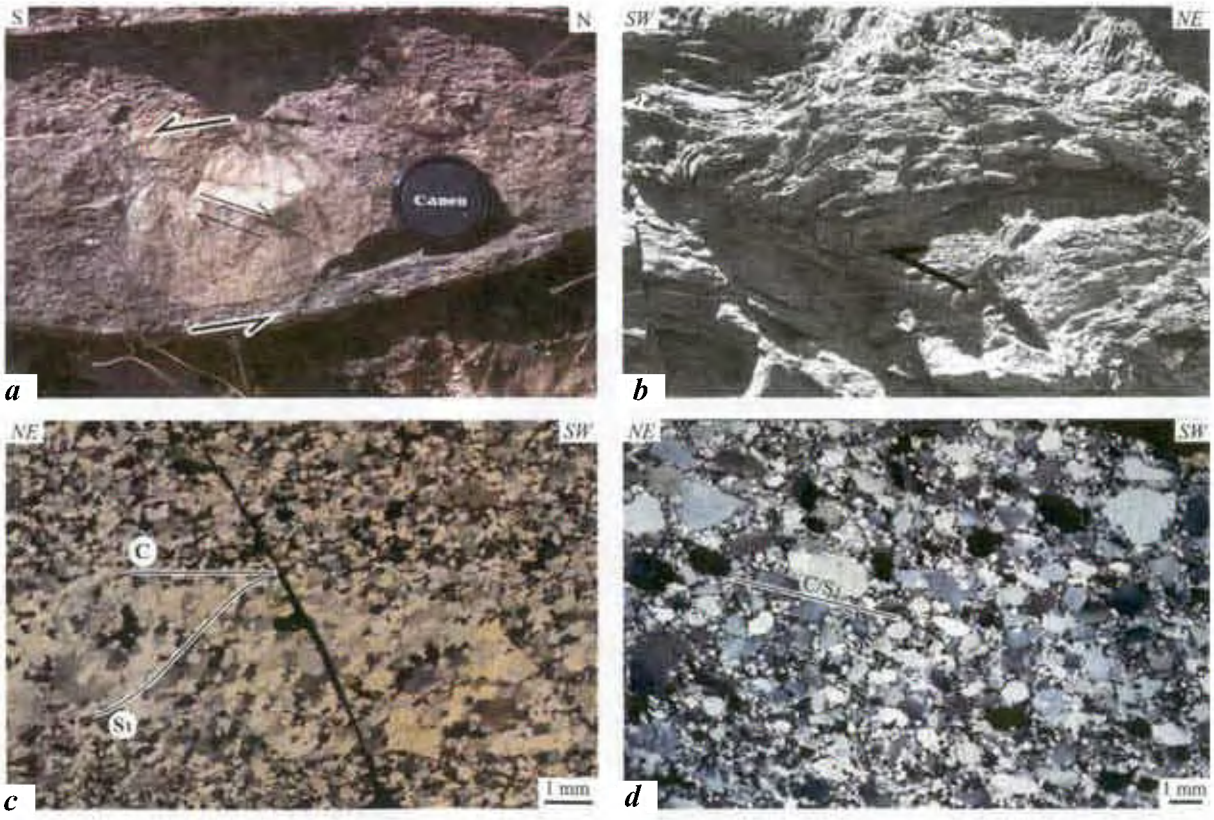

Figure 3. Shear fabric in the footwall of the JTZ. ***a***, Antithetically faulted (thin black arrow) quartzite pebble with overall top to SW shearing (arrows with white background). The style of deformation is analogous to the shearing of a deck of cards; ***b***, The synthetic shear zone in the footwall of the Jakhri Thrust with top to SW shearing; ***c***, Highly recrystallized quartzite with shape-preferred orientation of quartz and opaque grains (C) and oblique foliation (S_1) formed by quartz ribbon showing top to SW shear sense in the immediate vicinity of JT. (Top edge of the photomicrograph is parallel to the lineation direction); ***d***, Quartz mylonite, with abundant strained quartz porphyroclast, showing a faint shape preferred alignment in the farthest thrust zone. The quartz show core and mantle structure.

reference to foliation and stretching lineation in the footwall of the JTZ. Six samples (Figure 1, inset) with increasing distance from the Jakhri Thrust were analysed for the fluid inclusion studies. The petrographic observations and microthermic measurements on fluid inclusions have been carried out on doubly polished thin sections (~ 0.5 to 0.8 mm thickness) prepared from the rock wafer cut parallel to lineation and perpendicular to the S_1 foliation.

The size of fluid inclusions increases with increasing distance from the JTZ, viz. < 5 μm near the thrust to ~ 15–20 μm away. The fluid inclusions are tabular and stretched with pronounced necking near the thrust and are progressively lensoid away from the thrust. They lie mostly in trail with most trails being intragranular (terminating at quartz grain boundary). Most inclusions are bi-phasic (liquid and vapour); three-phase inclusions (solid + liquid + vapour) with halite crystals (Figure 4 *a*) restricted only to the lower part and mono-phase inclusions are restricted to the thrust zone. The fluid inclusions have been broadly categorized into three types on the basis of their occurrence and relation with the host rock microstructure in the JTZ – Types 1, 2 and 3.

Type 1 are the isolated and scattered primary inclusions restricted to quartz porphyroclasts in the lower part of the JTZ. They are large (~ 20 μm) and are mostly two- and three-phase inclusions with halite crystal constituting the solid phase (Figure 4 *a*). Many inclusions show negative crystal phase as well (Figure 4 *a*).

Type 2 are the most noticeable inclusion types occurring as FIP and lie oblique to the foliation at a higher angle (Figure 4 *b*, *c*). The size of inclusions is small in comparison to the type 1 inclusions. The inclusions are lensoid with length between ~ 5 and 20 μm and width ~ 5 μm. Individual fluid inclusions within the trail are aligned parallel to the foliation in the vicinity of JT, suggesting a strong finite strain. These trails trend due N–NW with reference to the horizontal foliation and stretching lineation (Figure 4 *d–f*). These inclusion trails are geometrically analogous to the extensional micro-fracture formed parallel to the $\acute{o}1$–$\acute{o}2$ plane of the stress field[7] formed during top to SW regional shearing. They are carbonic aqueous as well as aqueous in nature.

Type 3 are subvertical inclusion trails cross-cutting the type 2 inclusion trails (Figure 4 *c*) occurring at a high angle to the foliation trending due N–NE (Figure 4 *d–f*).

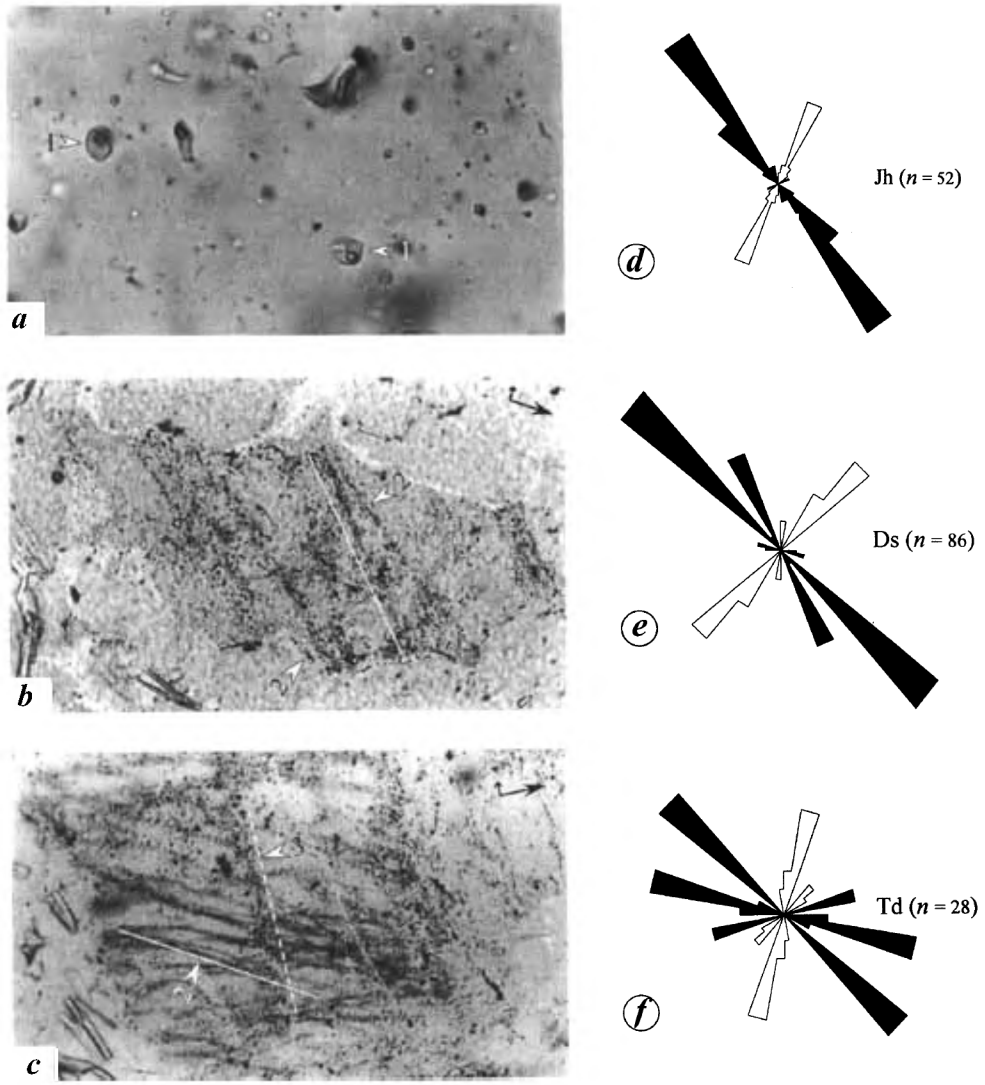

Figure 4. Fluid inclusion patterns in the quartz mylonite of the footwall of the JTZ. (The large arrow shows the lineation direction and the short arrow shows the top of the sample in ***a***, ***b***, ***c***). ***a***, Three-phase primary fluid inclusions (type 1) with halite crystal and negative crystal. Some stretched inclusions are also seen; ***b***, NW-trending type 2 FI trail in the intermediate zone lies within quartz porphyroclast. Please notice the abrupt termination of type 2 trails at the subgrain boundary; ***c***, Subhorizontal type 2 FI network with cross-cutting subvertical type 3 FI trail in the farthest zone; ***d–f***, N–NW trending type 2 (black) and NE-trending type 3 (hollow) fluid inclusion trail pattern with reference to the horizontal foliation and lineation in the JTZ increasing distance from the Jakhri Thrust.

These inclusions are usually very small in size (~ 5 μm) and aqueous in nature. These represent the latest phase of inclusion trails and are more pronounced in the farthest zone. Their geometry is analogous to the brittle–ductile top to NE extensional shearing in the JTZ.

Similar fluid inclusion trail pattern has been observed in the MCT zone of Nepal Himalaya where synthrusting *FI* trails lie oblique to the foliation and late inclusion trails are vertical or subhorizontal[7,10]. Since, type 2 inclusion trails are related to the thrusting along JT and expected to yield the deformation condition close to the peak *PT*, the microthermic measurements have been made on them. Further, the microthermic measurements on type 3 inclusions were not carried out due to their very small size.

Microthermic measurements of the FI have been performed on Linkam THMS-600 heating–freezing stage linked with TMS-92 programmed on Zeiss microscope. The stage has been calibrated at –56.6°C and –374.1°C using synthetic fluid inclusions[20]. The measured temperatures have a reproducibility of ±0.1–0.2°C at low temperatures and ±1–2°C at high temperatures. The composition, densities and isochores of the fluid inclusions have been calculated using the Flincor computer program[21] with the equations of state from Brown and Lamb[22]. Carbonic aqueous (CO_2–H_2O) and aqueous

(H_2O–NaCl) fluid inclusions have been distinguished in the type 2 FI trails.

The visually estimated volume percentage (%) of CO_2 in the CO_2–H_2O inclusions varies between 50 and 60%. The melting temperature of CO_2 (T_{mCO_2}) ranges between –56.4 and –57.4°C with the modal peaks at –56.6°C (Figure 5 *a*) suggesting a pure CO_2 phase with minor presence of CH_4. The homogenization temperature of CO_2 (T_{hCO_2}) ranges between 1.2 and 8°C with modal T_{hCO_2} decreases from ~6°C to ~3°C to ~1–2°C (Figure 5 *b*), suggesting an increasing CO_2 density away from the JT. The total homogenization temperature (T_{toth}) varies from 275 to 325°C (Figure 5 *c*) with a common modal peak between 280 and 290°C in the JTZ. The density of CO_2 phase and bulk density of inclusions, at minimum and maximum T_{hCO_2}, do not show significant variation. The little variation in density may be due to the leakage of H_2O in the high strain zone during re-equilibration[23].

The eutectic temperatures (T_e) of H_2O–NaCl inclusions in the JTZ vary from –21.2 to –23.5°C, suggesting NaCl–KCl–H_2O composition of the fluids[24]. The temperature of ice melting (T_{im}) of H_2O–NaCl inclusions varies between –1.7 and –12.8°C (Figure 5 *d*) with modal peak T_{im} increasing from –3°C to –7°C and –9°C with increasing distance in the JTZ. The modal wt% of NaCl (salinity) in type 1 inclusions is ~16 and between 5 and 14 in the type 2 inclusions with ~5–7 near the thrust, ~9.7–11.5 in the intermediate and 10–14 in the farthest zone. The modal bulk density of type 2 inclusions ranges from 0.89–0.84 g cm^{-3} and from 0.77 to 0.79 g cm^{-3} in the near and away from the thrust zone, respectively and from 0.7 to 0.72 g cm^{-3} in the type 1 inclusions. The salinity increase and the bulk density of H_2O–NaCl inclusion decrease away from the JT. The homogenization temperature (T_h) of H_2O–NaCl inclusions varies from ~260–280°C to 340–360°C (Figure 5 *e*) with increase in distance from the JT. The three-phase primary inclusions (type 1) with halite crystal in the farthest zone show T_h between 400 and 420°C. The high T_h is due to the presence of halite, which increases the homogenization temperature of the inclusion[24].

Isochores were calculated for CO_2–H_2O inclusions at peak modal T_{hCO_2} and for H_2O–NaCl inclusions at minimum and maximum T_{im} values[21,22]. Similar isochores of CO_2–H_2O inclusions in the JTZ suggest their final re-equilibration during single tectono-thermal event that may correspond to the early phase of exhumation after peak burial. The isochores of H_2O–NaCl inclusions in the JTZ show decreasing pressures away from the thrust (Figure 6), suggesting their progressive re-equilibration during different exhumation stages. In the absence of any characteristic mineral assemblage and the presence of chlorite in the JTZ, the chlorite zone metamorphism conditions have been plotted along with the isochores to get the limiting condition (Figure 6). The *PT* path of the isochores (Figure 6) suggests that the footwall has exhumed isothermally from a minimum depth of ~15–17 km, assuming lithostatic pressure conditions and ~2.8 g/cm^3 density of the rocks.

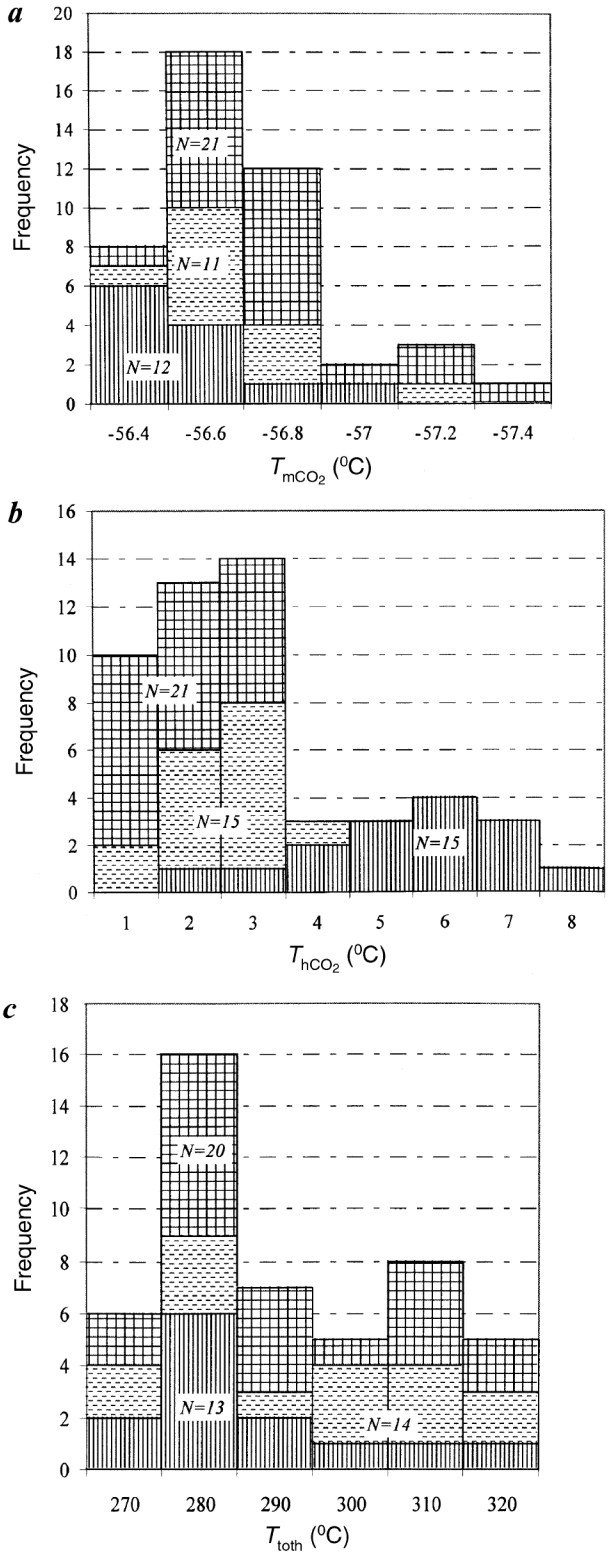

Figure 5. Composite histogram plot of (***a***), initial melting temperature of CO_2 (T_{mCO_2}); (***b***), homogenization temperature of CO_2 (T_{hCO_2}); (***c***), total homogenization temperature (T_{toth}) of CO_2–H_2O inclusions.

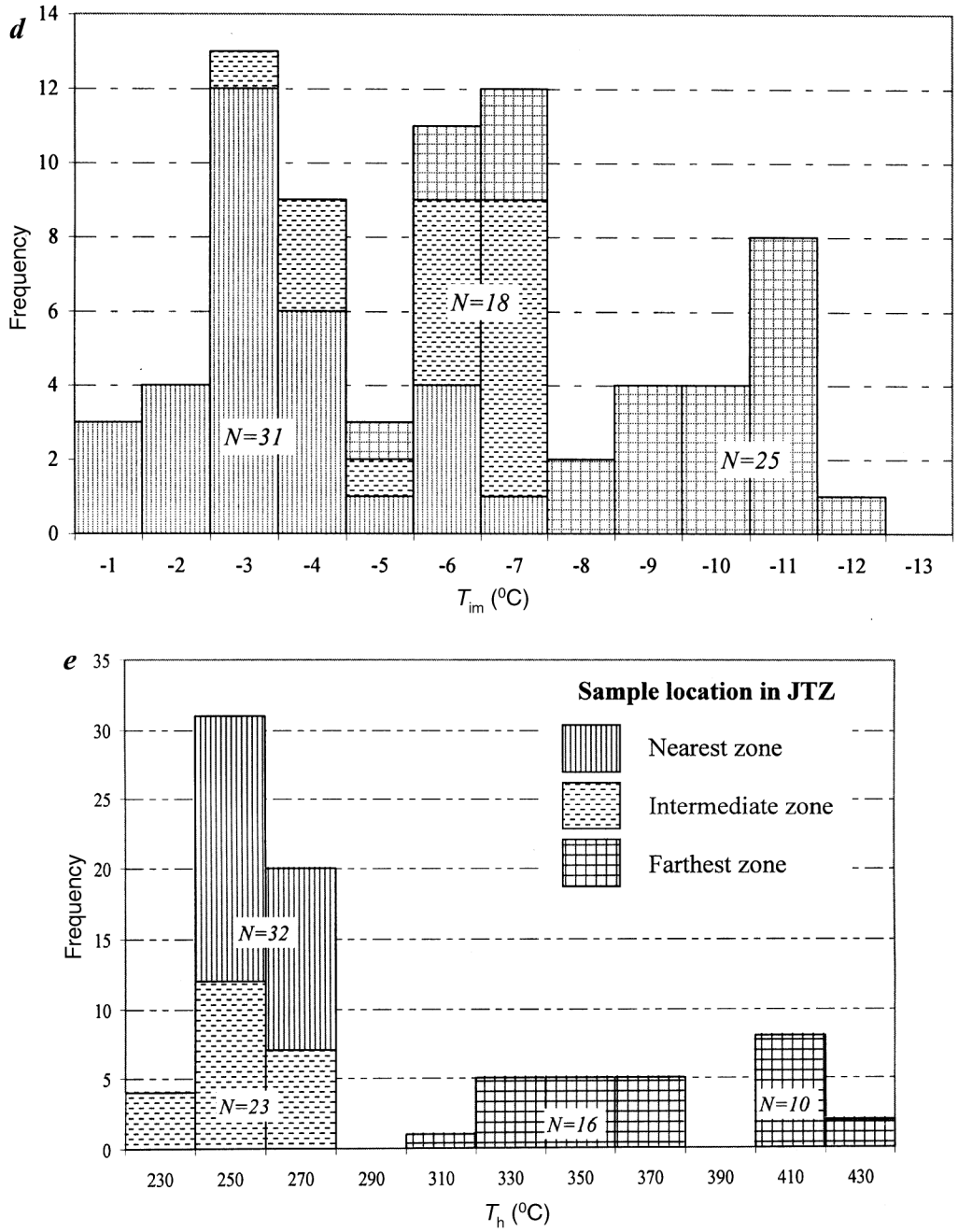

Figure 5. Composite histogram plot of (***d***), ice melting temperature (T_{im}) and (***e***) homogenization temperature (T_h) of H_2O–NaCl inclusions in the footwall of the JTZ. (*N*, number of inclusions measured).

The progressive change in the shape-preferred fabric of quartz and grain size in the shear zone are related to a progressive change in the strain rate, diffusional stress and temperature[25] and the fabric intensity is directly related to the finite strain[26]. In the JTZ, intensity of shape-preferred fabric in quartz–mylonite decreases and the size and content of quartz porphyroclast increases away from the thrust, suggesting a progressive decrease in finite strain. The deformation mechanism changes from the dominant subgrain rotation with feeble grain boundary migration (marked by quartz ribbon) to grain boundary migration to subgrain rotation (marked by core and mantle texture) away from the shear zone. The general presence of chlorite and T_h of fluid inclusions (which marks the lower temperature condition of entrapment and reequilibration[24]) suggest a temperature ~300–400°C, which is sufficient for the growth of recrystallization fabric and deformation of quartz.

A geometric relationship has been observed in the regional structure, microstructure and fluid inclusion trail

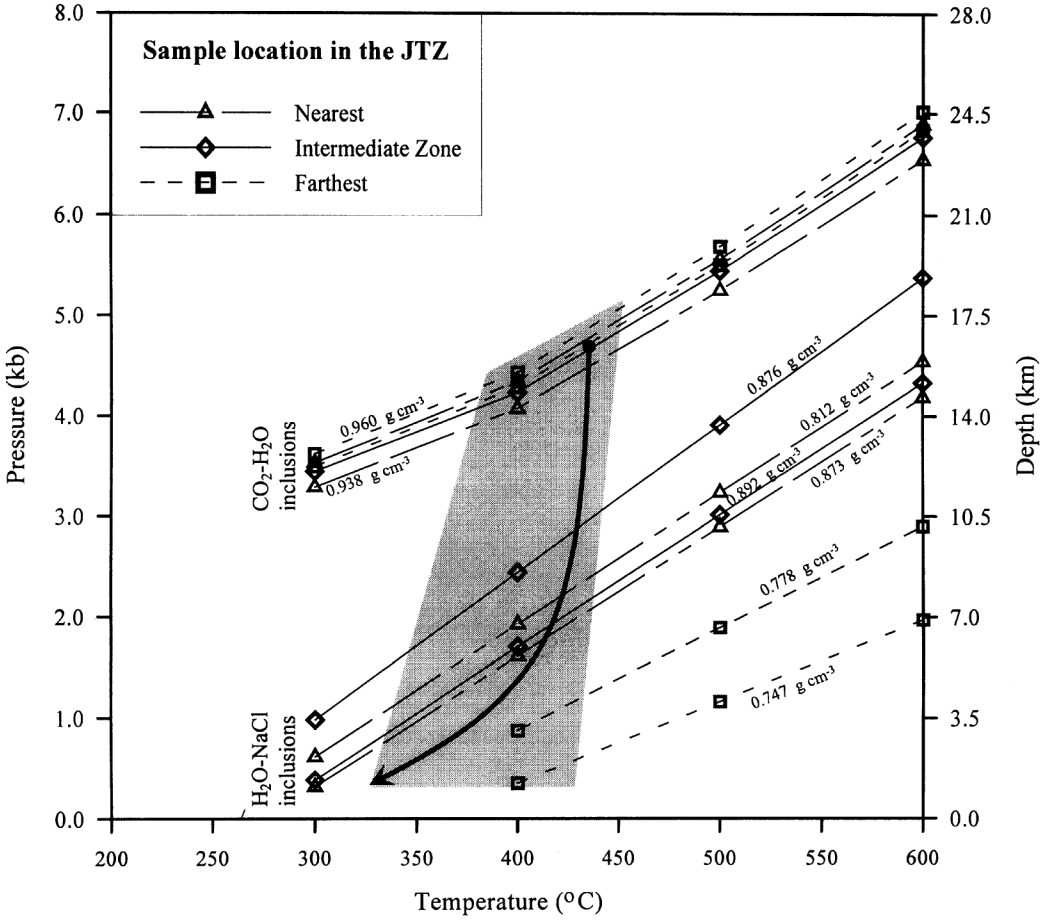

Figure 6. Isochore plot of the CO_2–H_2O and H_2O–NaCl fluid inclusions (along with density of the individual inclusion) in the footwall of the JTZ. The *PT* trajectory from the fluid inclusion isochores suggests an isothermal exhumation path in the lower greenschist facies condition (shaded area).

pattern in the JTZ and a schematic model has been proposed depicting the evolution of different fabric elements *vis-à-vis* JTZ (Figure 7). Ductile microstructure with top to SW shear sense is accompanied by the development of microcracks in the quartz resulting into type 2 inclusion trails (Figure 7 *a*). With increasing distance from JT, intensity of microstructure and type 2 FI trails decreases suggesting progressive decreases in shear intensity. SW compression is followed by brittle–ductile top to NE extensional shearing marked by extensional faulting and tension gashes (Figure 2 *b*), pull apart microstructures (Figure 7 *b*) and type 3 FI trails pattern (Figures 4 and 7 *b*). These fabrics have developed during gravity collapse of the hanging wall in the late evolution of the shear zone.

CO_2–H_2O and H_2O–NaCl fluid inclusions have been observed in the MCT zone of Nepal and Garhwal Himalaya shear zones[9–11]. The sources of these inclusions have invariably been traced from the host rock or metamorphic origin CO_2–H_2O fluid inclusions, which may have derived from the devolatilization of Lesser Himalayan sediments[7,10]. The T_{mCO_2} of the CO_2–H_2O inclusions in the JTZ show almost pure CO_2 phase and the density and salinity variation is very small. The homogenization temperature and isochore in the three structural zones of the footwall also show no marked variation. This suggests that the CO_2–H_2O inclusions in the JTZ might have derived from a common source, may be from the Shali Formation, which lies in the vicinity (Figure 1, inset), and have finally re-equilibrated during the same tectonic event that corresponds to the initial stages of exhumation after the peak burial.

It has been experimentally observed that the density of fluid decreases when fluid pressure is higher than confining pressure and vice versa and it may progressively reset to lower values with decreasing confining pressures during decompression or rapid exhumation[23,27]. The density changes of the H_2O–NaCl inclusions are due to changes in inclusion volume induced by plastic deformation of the host quartz grain[27] and diffusion or leakage of H_2O (ref. 28). The type 1 inclusions in the JTZ show a higher salinity and lower bulk density of H_2O–NaCl inclusions.

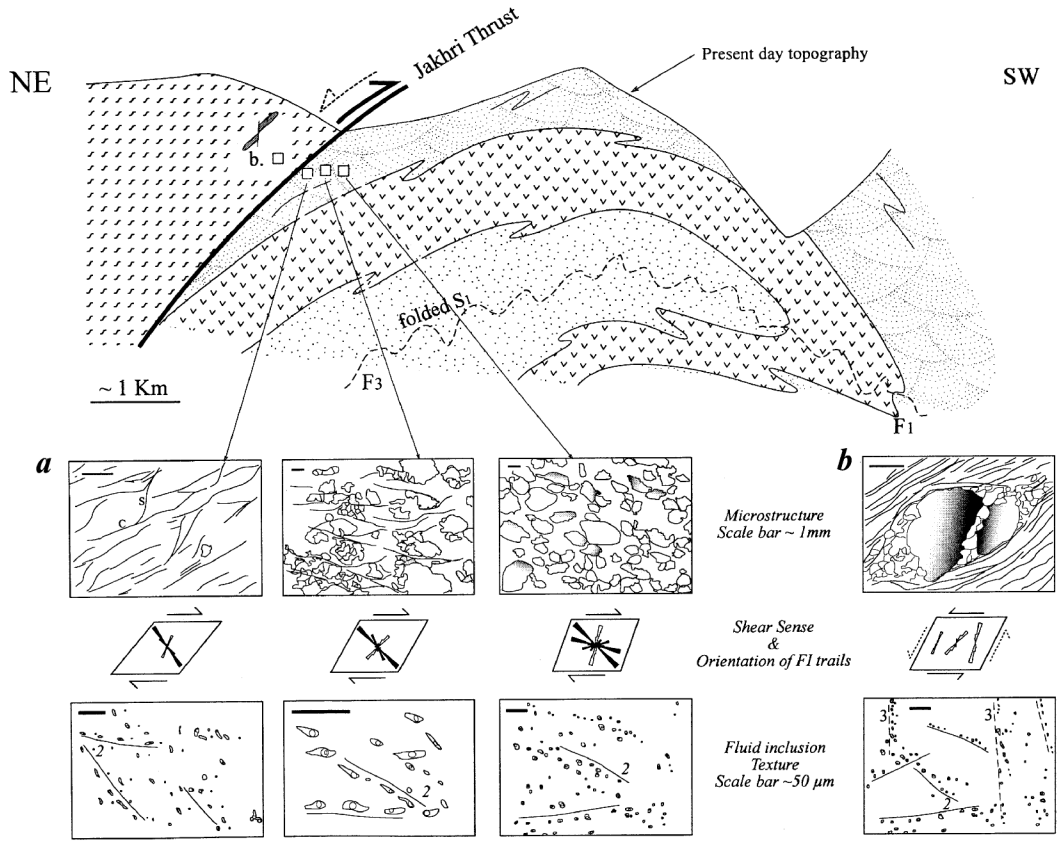

Figure 7. The schematic model representing the relationship of different structural elements (microstructure, shear sense, FI trail pattern and fluid inclusion texture) in the JTZ. ***a***, During top to SW thrusting the ductile shear fabric and type 2 inclusion trails have developed. The intensity of shearing decreases away from the thrust in the footwall; ***b***, At a later stage, top to NE tensional shearing resulting into the growth of extensional structures in the hanging wall and type 3 inclusion trails in the footwall.

The density of synkinematic type 2 of H_2O–NaCl inclusions increases towards the JT, suggesting an increase in internal pressure (P_i) (ref. 27). Near the JT, finite strain and strain rate are high as marked by ductile microstructures, leading to the decrepitation and fluid trapping into intragranular microcracks[7,29]. The fluid inclusion aligned parallel to the high strain direction has been observed in the JTZ. This process led to an instantaneous re-equilibration of the inclusions relative to its environmental P–T condition[7]. However in the farthest zone, H_2O–NaCl inclusions have re-equilibrated during exhumation (Figure 6).

The microstructure, mineral composition and fluid inclusions microthermometry suggest a peak 400–450°C geotherm preserved in the footwall of the JTZ. It is in direct contact with the 610°C geotherm[3] in the hanging wall, suggesting a break of ~ 150–200°C across the JTZ. The P–T trajectory of the fluid inclusion in the green schist facies condition suggests that the footwall of JTZ has exhumed isothermally from a depth of ~ 15–17 km, which is close to the depth of the Main décollement Surface (Fault) in the Lesser Himalayan zone[30]. The depth of exhumation along the JT suggests it to be a deeper thrust with limited outcrop exposure rather than a local tectonic boundary as perceived by Bhargava[17]. The cross-cutting relationship of JTZ with the folded Jutogh (Munsiari) nappe (Figures 1 and 2 *a*) suggests it to be a younger thrust and hence does not form a part of MCT zone as perceived by Sharma[15] and Virdi[16]. The fission track ages in the hanging wall of JTZ[1] suggest it to be active during < 5 Ma and hence younger than MBT, which was formed during ca. 10 Ma (ref. 2). This suggests that the JTZ is an out-of-sequence break-back thrust similar to the Tons Thrust in Garhwal Himalaya[30], which have been accommodating strain between MCT and MBT. The JTZ lies in the seismically active intermediate intensity earthquake zone of the inner Lesser Himalaya along the Himalaya arc, where Uttarkashi (1991) and Chamoli (1999) earthquakes (Figure 1) have occurred with the focal depth of ~ 17–18 km in the east. Microseismic observation in seismic network in the Kangra–Chamba region (Figure 1) suggests that the majority of events with 12–18 km foci depth lies in the same zone[31].

The result suggests that the Jakhri Thrust Zone (JTZ) is a SW propagating out-of-sequence thrust cutting across the folded Lesser Himalayan Crystalline nappe. It has

evolved in the lower green schist facies condition with a peak temperature of ~400–450°C suggesting a gap of ~150–200°C across the thrust. The *P–T* trajectory of the footwall of the JTZ suggests that it has exhumed isothermally from a depth of ~15–17 km. These results suggest that the JTZ is a deep-seated thrust, lying in the intermediate intensity earthquake zone of the Himalayan arc and probably is an imbrication on the main decollement fault between MBT and MCT. The study also highlights the significance of fluid inclusion trails pattern as tectonic markers and their utility in dealing with the exhumation history.

1. Jain, A. K., Kumar, D., Singh, S., Kumar, A. and Lal, N., *Earth Planet. Sci. Lett.*, 2000, **179**, 437–451.
2. Meigs, A. J., Burbank, D. W. and Beck, R. A., *Geology*, 1995, **23**, 423–426.
3. Vannay, J.-C., Sharp, Z. D. and Grasemann, B., *Contrib. Mineral. Petrol.*, 1999, **137**, 90–101.
4. Pêcher, A., Lespinasse, M. and Leroy, J., *Lithos*, 1985, **18**, 229–237.
5. Lespinasse, M. and Pêcher, A., *J. Struct. Geol.*, 1986, **8**, 169–180.
6. Cathelineau, M., Lespinasse, M., Bastoul, A. M., Bernard, L. and Leroy, J., *Mineral. Mag.*, 1990, **54**, 169–182.
7. Boullier, A. M., *J. Struct. Geol.*, 1999, **21**, 1229–1235.
8. Sauniac, S. and Touret, J., *Lithos*, 1983, **16**, 35–45.
9. Craw, D., *Lithos*, 1990, **24**, 137–150.
10. Boullier, A. M., Lanord, C. F., Dudessy, J., Adamy, J. and Champenois, M., *Contrib. Mineral. Petrol.*, 1991, **107**, 358–372.
11. Sachan, H. K., Sharma, R., Sahai, A. and Gururajan, N. S., *J. Asian Earth Sci.*, 2001, **19**, 207–221.
12. Miller, C., Klotzli, U., Frank, W., Thoni, M. and Grasemann, B., *Precambrian Res.*, 2000, **103**, 191–206.
13. Rao, D. R., Sharma, K. K. and Gopalan, K., *J. Geol. Soc. India*, 1995, **46**, 5–14.
14. Frank, W., Thoni, M. and Purtscheller, F., *Ecol. Geol. L'Himalaya*, 1977, **268**, 147–152.
15. Sharma, V. P., *Mem. Geol. Surv. India*, 1977, **106**, 235–403.
16. Virdi, N. S., *Him. Geol.*, 1980, **10**, 55–77.
17. Bhargava, O. N., *Him. Geol.*, 1980, **10**, 135–155.
18. Pandey, A. K., Unpublished Ph D thesis, Banaras Hindu University, India, 1999.
19. Pandey, A. K., Virdi, N. S. and Gairola, V. K., *Him. Geol.*, 2003, **24**, 1–21.
20. Bodnar, R. J. and Sterner, S. M., *Hydrothermal Experimental Techniques* (eds Barnes, H. L. and Ulmer, G. C.), Wiley & Sons, New York, 1987, pp. 423–457.
21. Brown, P. E., *Am. Mineralogist*, 1989, **74**, 1390–1393.
22. Brown, P. E. and Lamb, W. M., *Geochim. Cosmochim. Acta*, 1989, **53**, 1209–1221.
23. Bakker, J. R. and Jansen, B. H., *Nature*, 1990, **345**, 58–60.
24. Rodder, E., *Fluid Inclusion* (ed. Ribbe, P. H.), Mineralogical Society of America, 1984, vol. 12.
25. Ramsay, J. G., *J. Struct. Geol.*, 1980, **2**, 83–99.
26. Burg, J.-P. and Laurent, Ph., *Tectonophysics*, 1978, **47**, 15–42.
27. Sterner, S. M. and Bodnar, R. J., *J. Metamorph. Geol.*, 1989, **7**, 243–260.
28. Vityk, M. and Bodnar, R. J., *Contrib. Mineral. Petrol.*, 1995, **121**, 309–323.
29. Pêcher, A., *Tectonophysics*, 1981, **78**, 567–584.
30. Srivastava, P. and Mitra, G., *Tectonics*, 1994, **13**, 89–109.
31. Thakur, V. C., Sriram, V. and Mundepi, A. K., *Tectonophysics*, 2000, **326**, 289–298.

ACKNOWLEDGEMENTS. AKP acknowledges the financial support from CSIR, India in the form of research fellowship (Grant no.: 9/420(10)/94-EMR.I). Thanks are due to Dr H. K. Sachan for carrying out the microthermic measurement on the fluid inclusions. Prof. J. P. Burg, Drs B. Grasmann, D. Craw and an anonymous reviewer of the journal are acknowledged for useful comments on the earlier versions of the manuscript.

Received 19 August 2002; revised accepted 10 March 2003